Hydrodynamic effects in polydisperse charged colloidal suspensions at short times

G. Nägele, O. Kellerbauer, R. Krause, and R. Klein
Fakultät für Physik, Universität Konstanz, Postfach 5560, D-7750 Konstanz, Germany
(Received 11 November 1992)

The effect of combined intrinsic size and charge polydispersity and hydrodynamic interaction on the short-time dynamics in unimodal and bimodal suspensions of charged macroparticles is investigated. The first cumulant of the dynamic-scattering function is calculated based on a bimodal Schulz distribution for the particle sizes and charges. The influence of the solvent-mediated hydrodynamic interaction between the macroparticles is approximately described by a far-field expansion in terms of reciprocal distance r^{-1}, including terms up to order r^{-11}. The partial static-structure functions, which are required as an input, are obtained using the multicomponent-hypernetted-chain approximation. Our results are compared with data from dynamic-light-scattering experiments on binary mixtures of polystyrene spheres and on unimodal suspensions of charged silica particles. It is shown that both the intrinsic polydispersity and the hydrodynamic interaction significantly affect the measured first cumulant.

PACS number(s): 82.70.Dd, 61.20.Gy, 61.20.Lc

I. INTRODUCTION

A considerable amount of work has been done to investigate the microstructure and diffusion in one-component colloidal suspensions of spherical macroions [1,2]. Static light scattering (SLS) and dynamic light scattering (DLS) have been the main tools to obtain information about the static and dynamic properties of model suspensions, such as polystyrene spheres dispersed in water and silica particles dispersed in an organic solvent. As a result, there is an essentially quantitative understanding of monodisperse colloids, except for the effects of hydrodynamic interaction in the case of concentrated suspensions of particles with short-range potential interactions.

Much less is known, however, about colloidal mixtures and polydisperse suspensions due to their larger complexity. Colloidal mixtures show additional phenomena, e.g., a variety of microstructures and phase behavior, tracer diffusion, and interdiffusion, which do not exist in purely monodisperse systems.

In fact, in the process of synthesizing one-component suspensions, a certain amount of intrinsic polydispersity in the particle size is often unavoidable. If the particles are charged, it is expected that the size distribution gives rise to a corresponding charge distribution. The intrinsic size and charge polydispersity will affect the local ordering and the diffusion in the system.

Very recently, both static and dynamic properties of charged, two-component mixtures have been investigated experimentally by a variety of techniques [3–9]. Each component usually shows a combined intrinsic size and charge polydispersity and is more accurately represented by a multicomponent mixture characterized by an appropriate unimodal size distribution function.

The main objective of this work is to study the effect of the combined intrinsic size and charge polydispersity on the short-time dynamics in charged one- and two-component mixtures, as measured by the first cumulant of the dynamic scattering function. The first cumulant is affected both by static correlations, expressed by the measured static-structure factor $S_M(q)$ and by the solvent-mediated hydrodynamic interaction, which enters into the so-called apparent hydrodynamic function $H_M(q)$. Our present treatment is limited to an investigation of moderately highly charged suspensions with an overall volume fraction less than 0.1. The hydrodynamic function $H_M(q)$ is calculated approximately by considering only a two-particle stationary hydrodynamic interaction and by using a far-field expansion of the hydrodynamic mobility tensors of two unequal spheres, as provided by Jeffrey and Onishi [10]. The only additional input needed to obtain $H_M(q)$ and $S_M(q)$ is the knowledge of the partial radial distribution functions $g_{\alpha\beta}(r)$ and of the partial static structure factors $S_{\alpha\beta}(q)$. These static correlation functions are calculated by means of the hypernetted-chain approximation for colloidal mixtures. The macroions are described as charged hard spheres, interacting by a repulsive screened Coulomb potential of Derjaguin-Landau-Verwey-Overbeek (DLVO) type. The intrinsic size polydispersity in the one- and two-component systems is mimicked for each component respectively, by an optimized discretized representation of the unimodal continuous Schulz distribution of particle sizes, and the macroions are assumed to have constant surface charge density.

It will be shown that intrinsic polydispersity strongly affects the first cumulant. We also find that hydrodynamic interaction has a measurable effect on the first cumulant at small wave numbers, as compared to the position $q_{\max}$ of the main maximum of $S_M(q)$, even for moderately and highly charged particles at surprisingly low volume fractions.

The paper is organized as follows: In Sec. II, we describe our model of binary suspensions with intrinsic polydispersity. Pertinent dynamic-light-scattering relations for mixtures, relevant for obtaining the first cumulant of the dynamic-scattering function, are summarized in Sec. III. In Sec. IV, we give the details of our calculation of

the first cumulant in mixtures including hydrodynamic interaction. Section V contains our results which are compared with experimental data and with theoretical findings by Genz and Klein [11]. Our conclusions are summarized in Sec. VI.

II. MODEL SYSTEM OF INTRINSIC POLYDISPERSITY

We consider two-component colloidal suspensions of charged spheres. The two macroion components are labeled by the indices I and II, respectively. The components I and II are characterized by the volume fractions $\phi_{\rm I}$ and $\phi_{\rm II}$, the mean effective valences $\bar{Z}_{\rm I}$ and $\bar{Z}_{\rm II}$, and the mean diameters $\bar{\sigma}_{\rm I}$ and $\bar{\sigma}_{\rm II}$.

Each component has a certain size distribution around its mean diameter, depending on the chemical particle synthesis. It is well known that the measurable size distribution in one-component suspensions of polystyrene spheres can be well fitted using the two-parametric unimodal Schulz distribution, characterized by the mean diameter $\bar{\sigma}$ and the relative standard deviation s [12,13].

Therefore, the intrinsic size polydispersity of binary suspensions can be described by a continuous bimodal Schulz distribution of the form

$$p(\sigma)=x_{\rm I}p_S(\sigma;\bar{\sigma}_{\rm I},s_{\rm I})+(1-x_{\rm I})p_S(\sigma;\bar{\sigma}_{\rm II},s_{\rm II}) , \quad (2.1)$$

where

$$p_S(\sigma;\bar{\sigma},s)=\left[\frac{t+1}{\bar{\sigma}}\right]^{t+1}\frac{\sigma^t}{\Gamma(t+1)}\exp\left[-\frac{t+1}{\bar{\sigma}}\sigma\right] , \quad (t>0) \quad (2.2)$$

is the unimodal Schulz distribution function with relative standard deviation

$$s=\frac{[\langle\sigma^2\rangle-\bar{\sigma}^2]^{1/2}}{\bar{\sigma}}=[t+1]^{-1/2} . \quad (2.3)$$

The molar fraction of component I is given as $x_{\rm I}=\rho_{\rm I}/(\rho_{\rm I}+\rho_{\rm II})$ and $\rho_{\rm I}$ and $\rho_{\rm II}$ are the number densities of component I and II, respectively. It is the volume fractions $\phi_{\rm I}$ and $\phi_{\rm II}$ that can be determined experimentally, but not the number densities. Thus we express the number densities as

$$\rho_{\rm I,II}=\frac{6\phi_{\rm I,II}}{\pi\langle\sigma^3\rangle_{\rm I,II}} , \quad (2.4)$$

where $\langle\sigma^3\rangle_{\rm I}$ and $\langle\sigma^3\rangle_{\rm II}$ are the third moments taken with respect to the unweighted unimodal distribution functions $p_s(\sigma;\bar{\sigma}_{\rm I},s_{\rm I})$ and $p_s(\sigma;\bar{\sigma}_{\rm II},s_{\rm II})$ of the pure component I and II, respectively. Thus the molar fraction $x_{\rm I}$ and the number densities $\rho_{\rm I}$ and $\rho_{\rm II}$ depend on the volume fractions and the relative standard deviations of both components.

In a second step, the bimodal continuous distribution (2.1) is discretized by a $(N_{\rm I}+N_{\rm II})$-component histogrammatic representation

$$p(\sigma)=\sum_{\gamma=1}^{m}x_\gamma\delta(\sigma-\sigma_\gamma) , \quad (2.5)$$

with $m=N_{\rm I}+N_{\rm II}$. The weights x_γ and diameters σ_γ, where $\gamma=1,\ldots,N_{\rm I}$ refers to the $N_{\rm I}$ subcomponents which constitute component I are determined from the $2N_{\rm I}$ moment conditions

$$\sum_{\gamma=1}^{N_{\rm I}}x_\gamma(\sigma_\gamma)^l=x_{\rm I}\langle\sigma^l\rangle_{\rm I} , \quad (2.6)$$

with $l=0,1,\ldots,2N_{\rm I}-1$. Similarly, the corresponding parameters describing the $N_{\rm II}$ subcomponents of component II are obtained from

$$\sum_{\gamma=N_{\rm I}+1}^{m}x_\gamma(\sigma_\gamma)^l=(1-x_{\rm I})\langle\sigma^l\rangle_{\rm II} , \quad (2.7)$$

with $l=0,1,\ldots,2N_{\rm II}-1$. Instead of solving the nonlinear equations (2.5) and (2.6), we have used the equivalent Gauss-Laguerre method [13]. The numbers $N_{\rm I}$ and $N_{\rm II}$ have to be chosen appropriately, depending on the values for the relative standard deviations $s_{\rm I}$ and $s_{\rm II}$. In this work we consider samples with $s_{\rm I}=s_{\rm II}\le 0.3$. Then, it is sufficient to use a histogrammatic distribution with six subcomponents, i.e., $N_{\rm I}=N_{\rm II}=3$. This has been checked by varying the number of subcomponents. Figure 1 shows the histogrammatic representation of a typical binary mixture with $s_{\rm I,II}=0.1$.

In our further analysis we assume constant surface charge density for both components I and II. Explicitly, $Z_\gamma=\bar{Z}_{\rm I}[\sigma_\gamma/\bar{\sigma}_{\rm I}]^2$ for $\gamma=1,\ldots,N_{\rm I}$ and $Z_\gamma=\bar{Z}_{\rm II}[\sigma_\gamma/\bar{\sigma}_{\rm II}]^2$ for $\gamma=N_I+1,\ldots,m$.

The effective pair potential between the macroions is modeled as a hard-sphere potential plus a screened Coulomb potential of the form

$$\frac{u_{\alpha\beta}(r)}{k_BT}=\begin{cases}\infty, & r<a_\alpha+a_\beta\\ L_B\dfrac{Z_\alpha Z_\beta\exp[\kappa(a_\alpha+a_\beta)]}{(1+\kappa a_\alpha)(1+\kappa a_\beta)}\dfrac{\exp[-\kappa r]}{r}, & r>a_\alpha+a_\beta ,\end{cases} \quad (2.8)$$

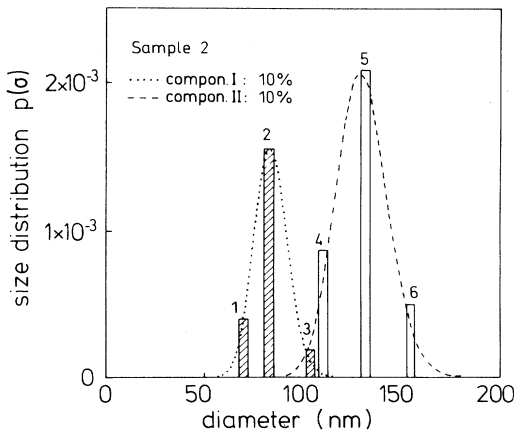

FIG. 1. Histogrammatic representation of the bimodal Schulz distribution describing the intrinsic size polydispersity of a binary macroion mixture (sample 2). $\{1,2,3\}\in$I and $\{4,5,6\}\in$II.

which is the repulsive part of the well-known DLVO potential for mixtures. Here, $a_\alpha=\sigma_\alpha/2$ is the radius of a α-type macroion ($\alpha=1,\ldots,m$), $L_B=e^2/\epsilon k_B T$ is the Bjerrum length, and

$$\kappa^2=4\pi L_B \rho_T \sum_{\alpha=1}^{m} x_\alpha |Z_\alpha| + \kappa_{\text{salt}}^2 , \tag{2.9}$$

where κ is the Debye-Hückel screening constant due to monovalent counterions and possible excess salt ions. The overall number density is $\rho_T=\rho_{\text{I}}+\rho_{\text{II}}$.

The partial radial distribution functions $g_{\alpha\beta}(r)$ and their Fourier transforms, the partial static structure factors $S_{\alpha\beta}(q)$, are calculated in this work using the multicomponent-hypernetted-chain (HNC) approximation. The HNC has been found to be quite useful as a fitting device for strongly coupled macroion mixtures [5].

III. DYNAMIC SCATTERING RELATIONS

In this section we briefly summarize some pertinent relations of the theory of dynamic light scattering in colloidal mixtures, which are required for our further discussion.

DLS experiments are often performed in the homodyne mode. Then the Siegert relation is used to deduce from the intensity autocorrelation function the normalized field autocorrelation function $g^{(1)}(q,t)$. The normalized field autocorrelation function is related to the so-called measured structure factor $S_M(q,t)$ by

$$g^{(1)}(q,t)=\frac{S_M(q,t)}{S_M(q)} , \tag{3.1}$$

where $S_M(q)=S_M(q,t=0)$. The measured dynamic structure factor of a m-component suspension is defined as [14]

$$S_M(q,t)=\frac{1}{\overline{f^2}(q)} \sum_{\alpha,\beta=1}^{m} (x_\alpha x_\beta)^{1/2} f_\alpha(q) f_\beta(q) S_{\alpha\beta}(q,t) . \tag{3.2}$$

Hence $S_M(q,t)$ is a superposition of $m(m+1)/2$ partial dynamic structure factors $S_{\alpha\beta}(q,t)$, weighted by the partial molar fractions x_α and the scattering amplitudes $f_\alpha(q)$ of α-type spheres. Here

$$\overline{f^2}(q)=\sum_{\gamma=1}^{m} x_\gamma f_\gamma^2(q) \tag{3.3}$$

is the second moment of the distribution of form amplitudes. The partial dynamic structure factors are defined as

$$S_{\alpha\beta}(q,t)=\langle c_{-\mathbf{q}}^{\alpha}(0) c_{\mathbf{q}}^{\beta}(t)\rangle , \tag{3.4}$$

where

$$c_{\mathbf{q}}^{\alpha}=\frac{1}{\sqrt{N_\alpha}} \sum_{l=1}^{N_\alpha} e^{i\mathbf{q}\cdot\mathbf{R}_l^\alpha} \tag{3.5}$$

is the Fourier component of density fluctuations of component α. N_α denotes the number of macroions of component α and the bracket indicates an equilibrium ensemble average. The magnitude of the scattering wave vector $\mathbf{q}$ is denoted as q, and $\mathbf{R}_i^\alpha(t)$ is the position vector at time t of the center of the ith macroion of component α. For the systems under study, the macroions or the refractive-index differences are small enough such that the Rayleigh-Gans-Debye approximation

$$f_\alpha(q)=3(n_p-n_s)a_\alpha^3 \frac{j_1(qa_\alpha)}{qa_\alpha} \tag{3.6}$$

for the scattering amplitude of a homogeneous spherical macroparticle of radius a_α and refractive index n_p is valid. The refractive index of the solvent is denoted by n_s.

The short-time dynamics obtained from DLS is usually characterized by an exponential decay of $S_M(q,t)$, expressed by the first cumulant $\Gamma_M^{(1)}(q)$, with

$$\Gamma_M^{(1)}(q)=-\lim_{t\to 0}\frac{\partial}{\partial t}\ln S_M(q,t) . \tag{3.7}$$

The short-time limit $t\to 0$ means that $\tau_B \ll t \ll \tau_{\text{I}}$, where we distinguish the momentum relaxation time $\tau_B=m/\xi^0$ from the structural relaxation time $\tau_{\text{I}}=a^2/D^0$, which is the time scale on which a macroion of mass m diffuses a distance equal to its radius a. Here $\xi^0=6\pi\eta_s a$ is the macroion friction coefficient, $D^0=k_B T/\xi^0$ is the free-particle diffusion coefficient, and η_s denotes the solvent shear viscosity. For a typical macroion radius of 100 nm, τ_B is of order 10^{-8} sec whereas τ_{I} is of order 10^{-3} sec, i.e., the short-time scale $\tau_B \ll t \ll \tau_{\text{I}}$ is usually well separated from the long-time scale $t \gg \tau_{\text{I}}$ [1]. There is an additional time scale related to the unsteady viscous solvent flow around the moving macroion. This time scale is characterized by the viscous relaxation time $\tau_H=a^2\rho_s/\eta_s$, where ρ_s is the mass density of the solvent. For typical colloidal suspensions we find $\tau_H \approx \tau_B$. Most of the recent DLS experiments are confined to delay times $t \gg \tau_B \approx \tau_H$. Then, solvent inertia effects can be neglected and the relaxation of only the macroion configuration is observed. This is referred to as Smoluchowski dynamics, in which the hydrodynamic interaction is described by the steady-state low Reynolds number creeping flow equation for an incompressible fluid [15].

IV. CALCULATION OF THE HYDRODYNAMIC FUNCTIONS

For delay times $t \gg \tau_B$, the N-particle Smoluchowski equation [16] is used to calculate equilibrium-configuration space-time correlation functions such as e.g., $S_{\alpha\beta}(q,t)$. The time evolution operator of any configuration space function is given by $\exp[\hat{O}_B t]$, where

$$\hat{O}_B(\mathbf{R}^N)=\sum_{\alpha,\beta=1}^{m} \sum_{i,j=1}^{N_\alpha,N_\beta} \left[\frac{\partial}{\partial \mathbf{R}_i^\alpha} - \frac{1}{k_B T}\frac{\partial U(\mathbf{R}^N)}{\partial \mathbf{R}_i^\alpha}\right] \cdot \mathbf{D}_{ij}^{\alpha\beta}(\mathbf{R}^N) \cdot \frac{\partial}{\partial \mathbf{R}_j^\beta} \tag{4.1}$$

is the backward or adjoint Smoluchowski operator [16]. Here $U(\mathbf{R}^N)$ is the potential energy of the suspension for the particle configuration $\mathbf{R}^N=(\mathbf{R}_1,\ldots,\mathbf{R}_N)$ of the total number of $N=\sum_{\gamma=1}^{m}N_\gamma$ macroions. The partial dynamic structure factor can be expressed as [16]

$$S_{\alpha\beta}(q,t)=\langle c_{-\mathbf{q}}^{\alpha}(0)e^{\hat{O}_B t}c_{\mathbf{q}}^{\beta}(0)\rangle \ . \tag{4.2}$$

From this equation and from Eqs. (3.2) and (3.7) we find for $\Gamma_M^{(1)}(q)$

$$\Gamma_M^{(1)}(q)=-\frac{1}{S_M(q)\overline{f^2}(q)} \times\sum_{\alpha,\beta=1}^{m}(x_\alpha x_\beta)^{1/2}f_\alpha(q)f_\beta(q)\langle c_{-\mathbf{q}}^{\alpha}\hat{O}_B c_{\mathbf{q}}^{\beta}\rangle \ . \tag{4.3}$$

In analogy to the case of monodisperse systems, we define an apparent q-dependent short-time diffusion coefficient $D_M(q)$ as

$$D_M(q)=\frac{\Gamma_M^{(1)}(q)}{q^2}=\frac{H_M(q)}{S_M(q)} \ , \tag{4.4}$$

where the apparent hydrodynamic function $H_M(q)$ is given by

$$H_M(q)=\frac{1}{\overline{f^2}(q)}\sum_{\alpha,\beta=1}^{m}(x_\alpha x_\beta)^{1/2}f_\alpha(q)f_\beta(q)H_{\alpha\beta}(q) \ . \tag{4.5}$$

The partial hydrodynamic functions $H_{\alpha\beta}(q)$ contain the effect of hydrodynamic interaction. The attribute "apparent" is used in order to emphasize that in mixtures $H_M(q)$ also depends on the single-particle scattering amplitudes $f_\alpha(q)$.

The $H_{\alpha\beta}(q)$ can be expressed by means of the backward operator $\hat{O}_B$ as

$$H_{\alpha\beta}(q)=\frac{1}{\sqrt{N_\alpha N_\beta}}\sum_{i,j=1}^{N_\alpha,N_\beta}\langle\hat{\mathbf{q}}\cdot\mathbf{D}_{ij}^{\alpha\beta}(\mathbf{R}^N)\cdot\hat{\mathbf{q}} \times\exp[i\mathbf{q}\cdot(\mathbf{R}_i^{\alpha}-\mathbf{R}_j^{\beta})]\rangle \ , \tag{4.6}$$

where $\hat{\mathbf{q}}=\mathbf{q}/q$, and $\mathbf{D}_{ij}^{\alpha\beta}(\mathbf{R}^N)$ denotes the translational diffusion tensors, relating the average velocity $\mathbf{V}_i^{\alpha}$ of macroion i of component α and the force $\mathbf{F}_j^{\gamma}$, on macroion j of component γ, i.e.,

$$\mathbf{V}_i^{\alpha}=\frac{1}{k_B T}\sum_{\gamma=1}^{m}\sum_{l=1}^{N_\gamma}\mathbf{D}_{il}^{\alpha\gamma}(\mathbf{R}^N)\cdot\mathbf{F}_l^{\gamma} \ . \tag{4.7}$$

The diffusion tensors depend in general on the positions of all N macroions, which explains the great complexity of the many-body hydrodynamic effects [17].

Without hydrodynamic interaction, $\mathbf{D}_{ij}^{\alpha\beta}$ reduces to $\mathbf{D}_{ij}^{\alpha\beta}=D_\alpha^0\delta_{\alpha\beta}\delta_{ij}\mathbf{1}$; in this case, $H_{\alpha\beta}(q)=\delta_{\alpha\beta}D_\alpha^0$, where $D_\alpha^0=k_B T/(6\pi\eta_s a_\alpha)$ is the Stokesian diffusion coefficient of a macroion of component α and 1 denotes the unit tensor. Then, $D_M(q)$ simplifies considerably to

$$D_M^0(q)=\frac{1}{S_M(q)\overline{f^2}(q)}\sum_{\gamma=1}^{m}x_\gamma f_\gamma^2(q)D_\gamma^0 \ , \tag{4.8}$$

where the short-time apparent diffusion coefficient only depends on quantities, which can be entirely determined from static-light-scattering experiments.

It is quite interesting to note that a part of $H_{\alpha\beta}(q)$ is related to the short-time tracer diffusion coefficient $D_\alpha^{s,\mathrm{short}}$ of a particle of component α. To see this, $H_{\alpha\beta}(q)$ is split into self- and distinct contributions, i.e.,

$$H_{\alpha\beta}(q)=\delta_{\alpha\beta}D_\alpha^{s,\mathrm{short}}+H_{\alpha\beta}^{d}(q) \ , \tag{4.9}$$

with

$$D_\alpha^{s,\mathrm{short}}=\langle\hat{\mathbf{q}}\cdot\mathbf{D}_{11}^{\alpha\alpha}\cdot\hat{\mathbf{q}}\rangle \ , \tag{4.10}$$

$$H_{\alpha\beta}^{d}(q)=\sqrt{N_\alpha N_\beta}\left[1-\frac{\delta_{\alpha\beta}}{N_\alpha}\right]\langle\hat{\mathbf{q}}\cdot\mathbf{D}_{12}^{\alpha\beta}\cdot\hat{\mathbf{q}}e^{i\mathbf{q}\cdot[\mathbf{R}_1^{\alpha}-\mathbf{R}_2^{\beta}]}\rangle \ . \tag{4.11}$$

In the expression for $H_{\alpha\beta}^{d}(q)$, a distinct representative pair of macroions $1\in\alpha$ and $2\in\beta$ has been chosen arbitrarily.

It can easily be shown from Eq. (4.10) that

$$D_\alpha^{s,\mathrm{short}}=\lim_{t\to 0}\frac{1}{6t}\langle[\mathbf{R}_1^{\alpha}(t)-\mathbf{R}_1^{\alpha}(0)]^2\rangle \ , \tag{4.12}$$

i.e., $D_\alpha^{s,\mathrm{short}}$ is essentially the initial slope of the mean-squared displacement (MSD) of an α-type macroion. Without hydrodynamic interaction, $D_\alpha^{s,\mathrm{short}}$ trivially reduces to $D_\alpha^{s,\mathrm{short}}=D_\alpha^0$, which can be understood from noting that at short times $\tau_B\ll t\ll\tau_I$, the MSD is not affected by the direct forces, since the configuration of the dynamic cage of next-neighbor macroions has not changed appreciably during the short time interval t. With hydrodynamic interaction, however, it is found that $D_\alpha^{s,\mathrm{short}}<D_\alpha^0$ due to the instantaneous hydrodynamic interaction of a macroion with its present neighbors.

In purely monodisperse systems, the initial decay of long-wavelength density fluctuations is described in terms of the short-time collective diffusion coefficient $D^{c,\mathrm{short}}$, defined as $D^{c,\mathrm{short}}=\lim_{q\to 0}D^{\mathrm{app}}(q)$. Here $D^{\mathrm{app}}(q)=D_M(q)$, provided the system is monodisperse.

In mixtures, however, all the possibly different scattering amplitudes $f_\alpha(q)$ enter into the expressions (4.4) and (4.5) for $D_M(q)$. Therefore, it is not $D_M(q)$ which describes the initial decay of fluctuations $c_{\mathbf{q}}=\sum_{\gamma=1}^{m}x_\gamma^{1/2}c_{\mathbf{q}}^{\gamma}$ of the total number density. Instead of $D_M(q)$, this decay is described by the q-dependent so-called number-number diffusion coefficient

$$D_{NN}(q)\equiv-\lim_{t\to 0}\frac{1}{q^2}\frac{\partial}{\partial t}\ln S_{NN}(q,t) =\frac{1}{S_{NN}(q)}\sum_{\alpha,\beta=1}^{m}(x_\alpha x_\beta)^{1/2}H_{\alpha\beta}(q) \ , \tag{4.13}$$

where

$$S_{NN}(q,t)=\sum_{\alpha,\beta=1}^{m}(x_\alpha x_\beta)^{1/2}S_{\alpha\beta}(q,t) \tag{4.14}$$

is the dynamic overall number-number structure factor, as defined by Bathia and Thornton [18]. $S_{NN}(q,t)$ and $S_M(q,t)$ are equal to each other only for mixtures with

pure charge polydispersity. For monodisperse systems $S_{NN}(q,t)=S_M(q,t)\equiv S(q,t)$ as well as $H_{NN}(q,t)=H_M(q,t)\equiv H(q,t)$. The short-time collective diffusion coefficient $D^{c,\text{short}}$ of monodisperse systems, has, in principle, to be distinguished from the long-time collective diffusion coefficient

$$D^{c,\text{long}}=-\lim_{t\to\infty}\lim_{q\to 0}\frac{1}{q^2}\frac{\partial}{\partial t}\ln S(q,t) \tag{4.15}$$

(with q^2t fixed), which can be measured from macroscopic gradient diffusion experiments or from DLS in the hydrodynamic limit. Notice that $t\to\infty$ means $t\gg\tau_I$. However, $D^{c,\text{short}}=D^{c,\text{long}}$ is strictly valid, provided that the direct forces and the hydrodynamic interaction are pairwise additive [2]. One might expect a similar equality to hold in mixtures with vanishing hydrodynamic interaction between $D_{NN}^{\text{short}}=\lim_{q\to 0}D_{NN}(q)$ and D_{NN}^{long}, where D_{NN}^{long} is defined by the right-hand side of Eq. (4.15) with $S(q,t)$ replaced by $S_{NN}(q,t)$. This equality $D_{NN}^{\text{long}}=D_{NN}^{\text{short}}$, however, does not hold in general. Instead, we consider the following linear combination:

$$S_{ff}(q,t)=\sum_{\alpha,\beta=1}^{m}(x_\alpha x_\beta)^{1/2}\xi_\alpha^0\xi_\beta^0 S_{\alpha\beta}(q,t) \tag{4.16}$$

of partial dynamic structure factors, where $\xi_\alpha^0=k_BT/D_\alpha^0$. We denote this linear combination as the dynamic friction-friction structure factor $S_{ff}(q,t)$. Then, for vanishing hydrodynamic interaction, it can easily be shown that the memory function, corresponding to $S_{ff}(q,t)$, vanishes faster than q^2, which leads to an exponential behavior of $S_{ff}(q,t)$ at small wave numbers for all times, i.e.,

$$S_{ff}(q,t)=\exp[-q^2D_{ff}t]S_{ff}(q)+O(q^4)\ , \tag{4.17}$$

with

$$D_{ff}=\lim_{q\to 0}\frac{1}{S_{ff}(q)}\sum_{\gamma=1}^{m}x_\gamma\xi_\gamma^0\ . \tag{4.18}$$

The dynamic function $S_{ff}(q,t)$ can be rewritten as $S_{ff}(q,t)=\langle c_{-\mathbf{q}}^f e^{\hat{O}_B t}c_{\mathbf{q}}^f\rangle$, where $c_{\mathbf{q}}^f=\sum_{\gamma=1}^m x_\gamma^{1/2}\xi_\gamma^0 c_{\mathbf{q}}^\gamma$ is the Fourier component corresponding to the center of friction $\mathbf{R}^f$, defined as $\mathbf{R}^f=\sum_{\gamma=1}^m\sum_{l=1}^{N_\gamma}\xi_\gamma^0\mathbf{R}_l^\gamma/(\sum_{\gamma=1}^m N_\gamma\xi_\gamma^0)$. The center of friction is a space point with respect to which the overall torque on all macroions due to the hydrodynamic friction forces $\xi_\gamma^0\mathbf{V}$ vanishes, i.e., $\sum_{\gamma=1}^m\sum_{l=1}^{N_\gamma}[\mathbf{R}_l^\gamma-\mathbf{R}^f]\times\xi_\gamma^0\mathbf{V}=\mathbf{0}$, provided that all macroions move with the same velocity $\mathbf{V}$. It follows from Eq. (4.17) that $D_{ff}^{\text{long}}=D_{ff}^{\text{short}}=D_{ff}$. Obviously, $D_{NN}\neq D_{ff}$ unless the friction coefficients of all components are equal to each other, which does only apply for charge polydispersity.

We now address the difficult task of calculating approximately the diffusion tensors $\mathbf{D}_{ij}^{\alpha\beta}$ and the hydrodynamic functions $H_{\alpha\beta}(q)$ as defined in Eq. (4.6). The diffusion tensors can be obtained in principle by solving the low-Reynolds-number creeping-flow equation for N spheres with appropriate boundary conditions on the surfaces. This is, however, an extremely difficult task. Not surprisingly, most theoretical work so far has been concentrated on dilute suspension, especially on model suspensions of monodisperse [19–24] and also polydisperse [16,25] hard spheres, where two-particle hydrodynamics is sufficient to first order in the overall volume fraction ϕ. At larger volume fractions (e.g., $\phi\geq 0.05$ for hard spheres), many-body interactions become important. Beenakker and Mazur [22–24] have provided an exact formal expression of the hydrodynamic function $H(q)$ in monodisperse suspensions of hard spheres, which is valid at arbitrary volume fractions. They have evaluated this expression approximately by using a renormalized density fluctuation expansion and their approximate $H(q)$ has been found to be an adequate description for moderately concentrated hard-sphere suspensions. More recently, Genz and Klein [11] have applied the renormalization approach of Beenakker and Mazur to monodisperse suspensions of moderately charged spheres, interacting by a screened coulomb potential of DLVO type. Their comparison with DLS data by Philipse and Vrij [26] on suspensions of charged silica spheres gives satisfactory agreement.

In contrast to monodisperse suspensions, much less is known about the effects of hydrodynamic interaction in polydisperse suspensions of charged spheres. Here, it becomes quite important to study the combined effects of intrinsic size and charge polydispersity and hydrodynamic interaction on the first cumulant $\Gamma_M^{(1)}(q)$ of the measured field auto-correlation function. As we already emphasized in the Introduction, we restrict ourselves in our analysis to colloidal mixtures of strongly to moderately charged spheres with low to moderate salinity and overall volume fractions less than 0.1. Then, the probability of two spheres getting close to each other is very small, due to the strong repulsion of the electric double layers. This can be seen from our HNC calculations of the partial radial distribution functions $g_{\alpha\beta}(r)$ of two spheres of type α and β, which are a distance r apart from each other. Therefore, we anticipate that the two-particle diffusion tensors give the dominant contribution.

Then, following the notations of Jones and Burfield [16] and assuming pairwise additivity, the translational diffusion tensors can be approximated as

$$\mathbf{D}_{ij}^{\alpha\beta}(\mathbf{R}^N)=\delta_{ij}^{\alpha\beta}\left[D_\alpha^0\mathbf{1}+\sum_{\gamma=1}^{m}\sum_{l=1}^{N_\gamma}{}'\,\mathbf{A}^{\alpha\gamma}(\mathbf{R}_i^\alpha-\mathbf{R}_l^\gamma)\right]+(1-\delta_{ij}^{\alpha\beta})\mathbf{B}^{\alpha\beta}(\mathbf{R}_i^\alpha-\mathbf{R}_j^\beta)\ , \tag{4.19}$$

where $\delta_{ij}^{\alpha\beta}=0$, whenever the indices $i\in\alpha$ and $j\in\beta$ refer to different spheres, and $\delta_{ii}^{\alpha\alpha}=1$. The prime on the double sum excludes the terms $\alpha=\gamma$ and $i=l$. The hydrodynamic tensors $\mathbf{A}^{\alpha\beta}(\mathbf{r})$ and $\mathbf{B}^{\alpha\beta}(\mathbf{r})$ can be expressed in terms of an expansion in the inverse distance r^{-1} between spheres of type α and β, by using the method of reflections [27–29]. Felderhof [27], e.g., has provided explicit expressions up to order r^{-7}. In our calculations, analytical expressions for $\mathbf{A}^{\alpha\beta}$ and $\mathbf{B}^{\alpha\beta}$ have been used up to order r^{-11}, as provided by Jeffrey and Onishi [10] for two freely rotating spheres of different radii a_α and a_β with stick boundary conditions on their surfaces. The expressions are rather lengthy and are collected in the Appendix.

The short-time dynamics obtained from DLS is usually

the distinct part $H^d_{\alpha\beta}(q)$ are expressed in terms of the hydrodynamic tensors as [16]

$$D^{s,\text{short}}_\alpha = D^0_\alpha + \rho_T \sum_{\gamma=1}^{m} x_\gamma \int d^3r [\hat{\mathbf{q}}\cdot \mathbf{A}^{\alpha\gamma}(\mathbf{r})\cdot\hat{\mathbf{q}}] g_{\alpha\gamma}(r) , \tag{4.20}$$

$$H^d_{\alpha\beta}(q) = \rho_T (x_\alpha x_\beta)^{1/2} \int d^3r [\hat{\mathbf{q}}\cdot\mathbf{B}^{\alpha\beta}(\mathbf{r})\cdot\hat{\mathbf{q}}] \times \cos(\mathbf{q}\cdot\mathbf{r}) g_{\alpha\beta}(r) . \tag{4.21}$$

Substituting the far-field expansion of $\mathbf{A}^{\alpha\beta}$ and $\mathbf{B}^{\alpha\beta}$ into Eqs. (4.20) and (4.21) and performing the angular integrals leads to rather lengthy expressions involving one-dimensional integrals which contain the radial distribution functions $g_{\alpha\beta}(r)$. These expressions are given in the Appendix, too. Jones and Schmitz [29] have provided similar results for $D^{s,\text{short}}_\alpha$ and, up to order q^2, also for $H^d_{\alpha\beta}(q)$, including terms up to r^{-7}.

In performing the integrals in Eqs. (4.20) and (4.21), one obtains rapid convergence, since in contrast to uncharged spheres, where the $g_{\alpha\beta}(r)$ are large at contact, these functions are practically zero for small separations due to the electrostatic repulsion. Therefore, it seems unnecessary to consider lubrication theory [10] of nearly touching spheres.

For completeness, we finally give the results for $D^{s,\text{short}}$ and $D^{c,\text{short}}$ obtained from the reflection method for monodisperse hard-sphere suspensions to first order in ϕ. It is found that $D^{s,\text{short}} = D^0[1-\alpha^s\phi]$ and $D^{c,\text{short}} = D^0[1+\alpha^c\phi]$ with $\alpha^s = 1.73$, $\alpha^c = 1.56$ including terms up to order r^{-7}, and $\alpha^s = 1.79$, $\alpha^c = 1.44$ including terms up to order r^{-11}. Recent calculations of Cichocki and Felderhof [21], taking into account a large number of reflections, lead to $\alpha^s = 1.831$ and $\alpha^c = 1.454$.

V. RESULTS

In the first part of this section we discuss our theoretical and experimental findings on the first cumulant of the measured dynamic structure factor $S_M(q,t)$ as applied to dilute binary suspensions of strongly charged spheres.

DLS and SLS experiments have been performed on twelve different binary suspensions of charged polystyrene spheres, mixed together from two well-characterized one-component batches I and II, with average diameters $2\bar{a}_\text{I} = 84$ nm and $2\bar{a}_\text{II} = 130$ nm, respectively. The total volume fraction $\phi_T = \phi_\text{I} + \phi_\text{II}$ of all twelve samples has been kept approximately constant and the binary suspensions are located within the homogeneous liquid phase. The samples have been treated by mixed-bed ion exchange resins, such that essentially all excess ions have been removed. In a recent publication by Krause *et al.* [5], the static properties of all twelve samples have been characterized in great detail by SLS data of $S_M(q)$, as well as by Monte Carlo computer simulations and the results of integral equation theories, using the extended rescaled mean spherical and the hypernetted-chain approximations and the Rogers-Young closure scheme. The values of the mean effective valences $\bar{Z}_\text{I}, \bar{Z}_\text{II}$ entering the effective pair potential, Eq. (2.7), were determined by fitting the static structure factor of the pure components I and II, and they were kept constant for the mixtures. It was shown that it is necessary to take intrinsic polydispersity into account in order to get an optimal description of the SLS data.

TABLE I. Partial volume fractions $\phi_{\text{I,II}} = (4\pi/3)\rho_{\text{I,II}} a^3_{\text{I,II}}$ (units of 10^{-4}) of the samples 2, 3, 9, and 12 under study. The values are taken from Ref. [5].

Fraction \ Sample	2	3	9	12
ϕ_I	0.53	0.95	3.85	6.2
ϕ_II	4.05	3.6	1.35	0

The latter have been supplemented quite recently by DLS data of the first cumulant of $S_M(q,t)$. As a selection, we will only discuss the data of samples 2, 3, 9, and 12. The system parameters characterizing these samples are listed in Tables I and II. Notice that samples 2, 3, and 9 are binary mixtures whereas sample 12 consists only of type-I spheres. (for a complete parameter list of all twelve samples, see Tables 1 and 2 in Ref. [5]).

We describe the intrinsic polydispersity in sizes and charges by an optimized histogrammatic bimodal Schulz distribution, as explained in Sec. II. Here, each component I and II is replaced by a histogram of three subcomponents, respectively (i.e., $N_\text{I} = N_\text{II} = 3; m = 6$) and the standard deviations s_I, s_II are varied from 0 to 0.3. The radial distribution functions $g_{\alpha\beta}(r)$, which are required as a static input in Eqs. (4.20) and (4.21), are obtained by numerically solving the HNC integral equation.

Our experimental and theoretical results for samples 3 and 9 are shown in Figs. 2(a) and 2(b), where the apparent short-time diffusion coefficient $D_M(q)$ is compared to the one calculated without hydrodynamic interaction, $D^{(0)}_M(q)$. The major difference between the two is seen to be a reduction or retardation of the diffusion due to the presence of hydrodynamic interaction for wave numbers $q < q_\text{max}$, where q_max is the position of the main peak of $S_M(q)$ [$S_M(q_\text{max}) \approx 1.6$ and 1.75 for samples 3 and 9, respectively]. The effect is most pronounced at $q = 0$, where the reduction is more than 10%. Both figures contain the theoretical results for $D_M(q)$ and $D^0_M(q)$ for vanishing intrinsic polydispersity and for a rather modest amount of intrinsic polydispersity with $s_\text{I,II} = 0.1$.

It is seen that the inclusion of intrinsic polydispersity further decreases $D_M(q)$ for $q < q_\text{max}$. For $q \geq q_\text{max}$, the differences between $D_M(q)$ and $D^0_M(q)$ become negligibly small for the systems under study. In order to make

TABLE II. Parameters characterizing macroions of the pure components I and II. The values are taken from Ref. [5]. The effective valences $\bar{Z}^\text{HNC}_\text{I,II}$ are used in our calculations of $S_M(q)$ and $D_M(q)$.

Component	$2a$ (nm)	$\bar{Z}^\text{HNC}$	$\bar{Z}^\text{MC}$
I	84	438	330
II	130	323	280

these features more transparent, the normalized hydrodynamic function $D_M(q)/D_M^0(q)$ calculated for the parameters of sample 12 is shown in Fig. 3 for different degrees of polydispersity $s_I=0-0.3$. Notice that the contribution due to $S_M(q)$ is divided out here. At large wave numbers, where $S_M(q)\approx 1$, it follows from Eqs. (4.4) and (4.8) that

$$\frac{D_M(q)}{D_M^0(q)} \approx \frac{\sum_{\gamma=1}^{m} x_\gamma f_\gamma^2(q) D_\gamma^{s,\text{short}}}{\sum_{\gamma=1}^{m} x_\gamma f_\gamma^2(q) D_\gamma^0} . \tag{5.1}$$

It is important to observe from Fig. 3 in the case of sample 12 (and this applies to all other samples) that $\lim_{q\to\infty} D_M(q)/D_M^0(q)=1$, i.e., that $D_\alpha^{s,\text{short}}=D_\alpha^0$. Thus the self-part of $H_{\alpha\alpha}(q)$, which is the short-time tracer diffusion coefficient $D_\alpha^{s,\text{short}}$, is practically unchanged by the hydrodynamic interaction which is in contrast to the behavior of $D_M(q)/D_M^0$ at small wave numbers. The reason for this behavior follows from the structure of

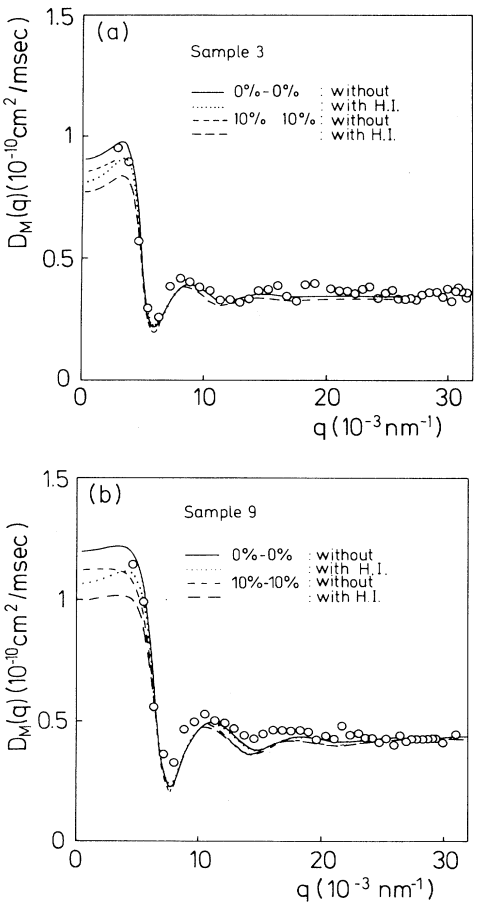

FIG. 2. (a) Apparent short-time diffusion coefficient $D_M(q)$ of sample 3, for standard deviations $s_I=s_{II}=0.1$. Comparison of experimental data (open circles) with pairwise additivity theory (with and without hydrodynamic interaction). (b) Same as in (a), but for sample 9.

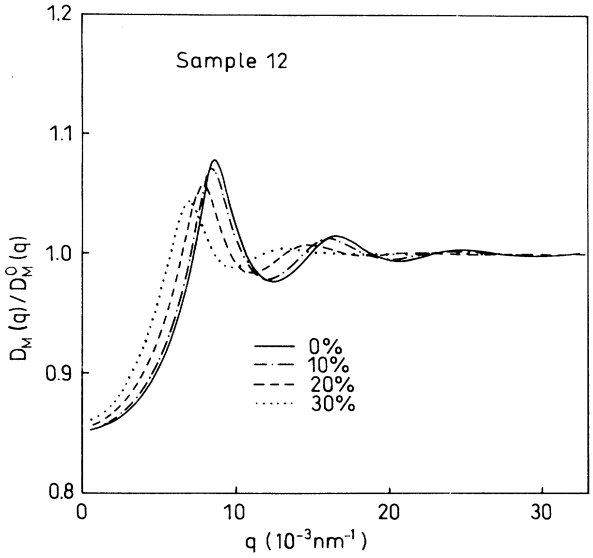

FIG. 3. Normalized hydrodynamic function $D_M(q)/D_M^0(q)$ of sample 12, with polydispersities $s_I=0.0$, 0.1, 0.2, and 0.3. $D_M^0(q)$ is the apparent diffusion coefficient without hydrodynamic interaction.

Eqs. (4.4), (4.5), (4.20), and (4.21) and our explicit far-field expressions for the hydrodynamic tensors $\mathbf{A}^{\alpha\beta}$ and $\mathbf{B}^{\alpha\beta}$. The radial distribution functions $g_{\alpha\beta}(r)$ are practically zero at distances $r<5(a_\alpha+a_\beta)$. As a consequence only the leading contribution of order r^{-1} in the far-field series, which is the so-called Oseen part, contributes significantly to $H_M(q)$. The Oseen part, however, enters only into $\mathbf{B}_{\alpha\beta}$ and $H_{\alpha\beta}^d(q)$. The leading contribution to $D_\alpha^{s,\text{short}}$ is of order r^{-4} and therefore negligibly small for the systems under study.

As a conclusion, it has to be emphasized that the frequently used argument, according to which hydrodynamic interaction is negligible for very dilute suspensions of strongly charged particles, holds only for the self-part which represents short-time diffusion. For the same systems, hydrodynamic interaction leads, however, to a significant effect on the first cumulant for small wave numbers $q<q_{\max}$. A precise measurements of these effects is difficult because of large uncertainties in determining the first cumulant at very small wave numbers.

The consideration of higher-order cluster contributions to the hydrodynamic interaction does not alter these statements since, e.g., according to Mazur and van Saarloos [28], three-body terms in $\mathbf{D}_{\alpha\beta}$ and $\mathbf{D}_{\alpha\alpha}$ first appear in order r^{-4} and r^{-7}, respectively, and are therefore expected for the dilute systems under consideration to be negligibly small. Figures 2(a) and 2(b) indicate that the agreement between theory and DLS data deteriorates with increasing polydispersity. However, as discussed in detail in Ref. [5], polydispersity reduces the value of the peak height and shifts the peak position to lower q. In order to recover and even to improve the good fit of the experimental $S_M(q)$ using HNC, we have to increase the values of the partial volume fractions as well as the values of the

effective valences. According to Ref. [5], a polydispersity of $s_{I,II}=0.1$ together with $\bar{Z}_{I,II}=540,400$ leads to HNC structure factors, which reproduce with high accuracy the experimental $S_M(q)$ (cf. Fig. 8 in Ref. [5]). Figure 4 shows that also the fit of the experimental $D_M(q)$ is slightly improved, although the fit is not as good as for $S_M(q)$.

We now continue to discuss the form of the normalized hydrodynamic function $D_M(q)/D_M^0(q)$, as shown for sample 12 in Fig. 3. Sample 12 solely consists of type-I spheres. Then for $s_{I,II}=0$, $D_M(q)/D_M^0(q)$ reduces to $H(q)/D^0$, with $D^0=k_BT/6\pi\eta_s a_I$. Intuitively, one might expect that hydrodynamic interaction always causes a slowing down of the particle dynamics [1,2], e.g., $H(q)/D^0<1$ should hold at all wave numbers. A relatively large hydrodynamic resistance [i.e., small $H(q)/D^0$] is expected at small wave number $q \ll q_{max}$, since for $q\rightarrow 0$ the density fluctuations described by $S(q,t)$, are relaxed by collective motion of neighboring particles in the same direction. Near the main peak of $S(q)$, i.e., at $q\approx q_{max}$, $S(q,t)$ is mainly relaxed by motion of particles in opposite directions, and one expects the hydrodynamic resistance to be smaller and thus $H(q)/D^0$ to be larger (but still smaller than unity). Indeed, this predicted behavior has been verified both experimentally [30] and theoretically [22–24] in the case of monodisperse hard-sphere suspensions. From Fig. 3 it is seen, however, that in charged suspensions $H(q)/D^0$ actually gets larger than unity near q_{max}, which contradicts the assumption that hydrodynamic interaction always causes hindrance of particle dynamics. The fact that $H(q)/D^0>1$ in monodisperse charged suspensions near q_{max} has been observed before both experimentally [26] and theoretically [11,31] by several groups. Figure 3 illustrates that the same behavior can be expected in charged polydisperse suspensions for $D_M(q)/D_M^0(q)$. It should be noted that the oscillations in $D_M(q)/D_M^0(q)$ are

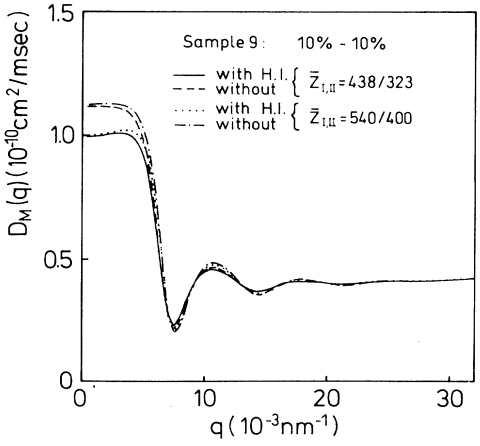

FIG. 4. $D_M(q)$ of sample 9, calculated for two sets of parameters. The first parameter set is given in Tables I and II. The second parameter set with $\phi_{I,II}=4.03\times10^{-4}$, 1.41×10^{-4}; $\bar{Z}_{I,II}=540,400$ is taken from Table 3 of Ref. [5] and gives an excellent HNC fit of the experimental $S_M(q)$.

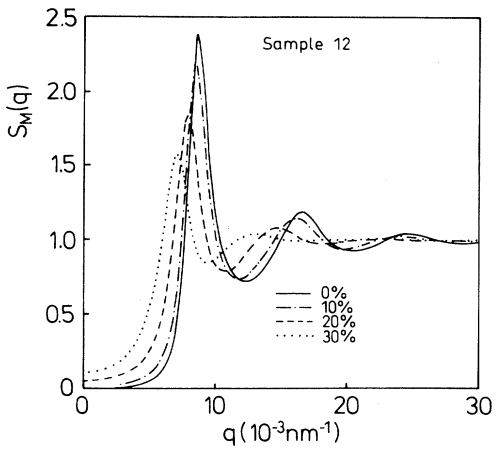

FIG. 5. HNC results for the measured static structure factor $S_M(q)$ of sample 12. Standard deviations as indicated in the figure. System parameters are given in Tables I and II.

reduced and washed out with increasing polydispersity, and this behavior is shared by the static measured structure factor $S_M(q)$, as can be seen from Fig. 5.

As discussed already in Sec. IV, the initial decay of the total number density is described by $D_{NN}(q)$ instead of $D_M(q)$. We show results for $S_{NN}(q)$ and $D_{NN}(q)/D_{NN}^0(q)$ in Figs. 6 and 7, respectively, to compare them with the corresponding measurable quantities $S_M(q)$ and $D_M(q)$. The number-number structure factor $S_{NN}(q)$ is a measure of the linear response of the system to an external perturbation which couples to the total number density, irrespective of the amount of charge on the different components. The concentration ordering described by $S_{NN}(q)$ is found to be reduced with increasing polydispersity s [12]. In particular, with increasing polydispersity there is a strong increase of $S_{NN}(q)$ at small wave numbers q (cf. Fig. 6), with values exceeding the ones of $S_M(q)$ for the same system considerably (cf. Fig. 5). The oscilla-

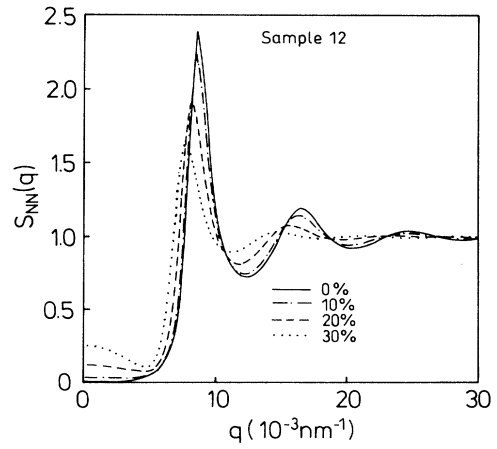

FIG. 6. HNC results for the static number-number structure factor $S_{NN}(q)$ of sample 12, corresponding to Fig. 5.

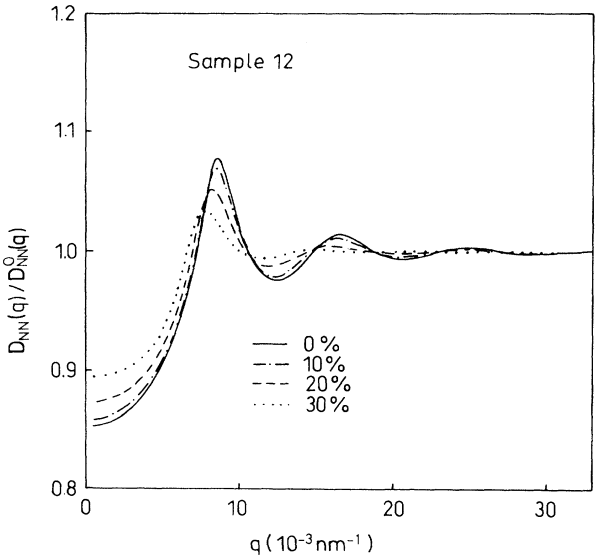

FIG. 7. Normalized number-number diffusion coefficient $D_{NN}(q)/D^0_{NN}(q)$ of sample 12, corresponding to Fig. 3. $D^0_{NN}(q)$ is the q-dependent number-number diffusion coefficient without hydrodynamic interaction.

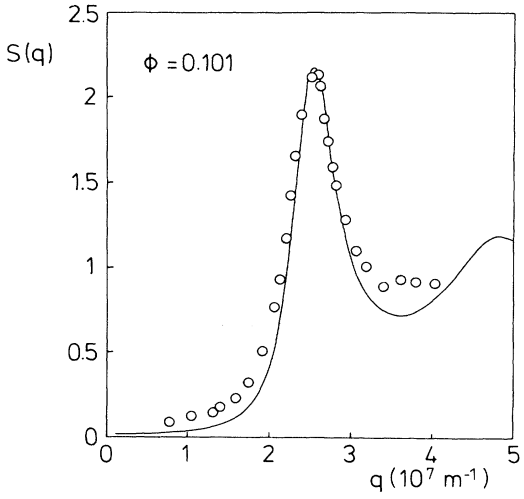

FIG. 8. Static structure factor of a monodisperse suspension of charged silica spheres. Open circles indicate the experimental results of Philipse and Vrij [26], the full line is the HNC fit. The system parameters used in the HNC calculation are $\phi=0.101$, $Z^{\mathrm{HNC}}=107$, $a=80$ nm, $\kappa a=1.7$, and $\epsilon=10$.

tions of $D_{NN}(q)/D^0_{NN}(q)$ are reduced with growing polydispersity. Furthermore, $D_{NN}(q)/D^0_{NN}(q)$ exhibits a somewhat stronger variation with q than $D_M(q)/D^0_M(q)$ in Fig. 3. It can also be seen that $D_{NN}(q)/D^0_{NN}(q)$ is more sensitive to polydispersity at small q, but the shift of its main peak to smaller q is less pronounced. The main features of $D_{NN}(q)/D^0_{NN}(q)$, as compared to those of $D_M(q)/D^0_M(q)$, are therefore similar to those of $S_{NN}(q)$ as compared to $S_M(q)$.

Up to this point we have investigated the short-time dynamics of polydisperse dilute charged suspensions. We will now compare our theoretical results with recent measurements of the hydrodynamic function $H(q)$ in monodisperse systems of coated charged silica spheres with radius of 80 nm, immersed in an optically matching mixture of ethanol and toluene [26]. The volume fraction ϕ of these samples is inside the range 0.009–0.101, which is much larger than the total volume fraction $\phi_T \approx 10^{-3}$ of the dilute deionized suspensions discussed before.

Figures 8 and 9 show a comparison of the SLS data for the static structure factor $S(q)$ for the most concentrated samples with $\phi=0.101$ and 0.079, and the structure factor calculated from the HNC closure. The parameters are $Z^{\mathrm{HNC}}=107$, $\epsilon=10$, and $\kappa a=1.7$, where κ has been kept fixed to this value independent of ϕ. Genz and Klein [11] used the thermodynamically self-consistent Rogers-Young (RY) closure to calculate $S(q)$ for the most concentrated system with $\phi=0.101$. Their result for $S(q)$ is identical to ours by using a slightly smaller valency of $Z^{\mathrm{RY}}=100$, all other parameters being the same.

The fit of the experimental $S(q)$ is seen from Figs. 8 and 9 to be quite satisfactory. The differences between experimental data and the HNC result at small q may be due to slight polydispersity.

Our purpose here, however, is not to obtain an optimal fit of the experimental $S(q)$ and $H(q)$, but to test our calculations of $H(q)$, which are based on the pairwise additivity assumption of the hydrodynamic interaction and the far-field expansion versus the more elaborate renormalization approach of Beenakker and Mazur [22–24], as applied by Genz and Klein [11] to more concentrated monodisperse charged suspensions. In Fig. 10, our result for the normalized hydrodynamic function $H(q)/D^0$ is compared, for the most concentrated system, in which case hydrodynamic interaction is most important, to the experimental data and the result of Genz and Klein. The shape of the experimental $H(q)$ (open circles) is equally

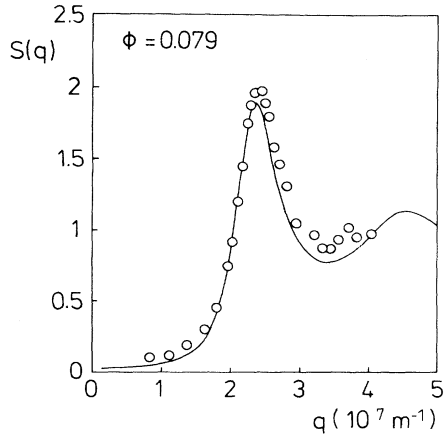

FIG. 9. Same as in Fig. 8, but with $\phi=0.079$.

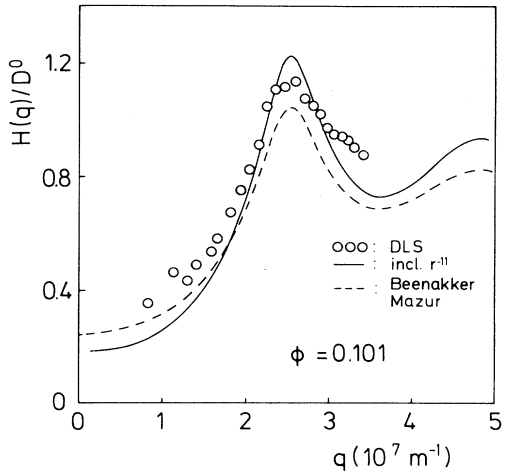

FIG. 10. Normalized hydrodynamic function $H(q)/D^0$. The continuous line is the result of the pairwise additivity theory, with static HNC input for $g(r)$. The dashed line is the result for the renormalized density fluctuation expansion of Beenakker and Mazur, as calculated by Genz and Klein [11]. Open circles show the experimental results of Philipse and Vrij [26].

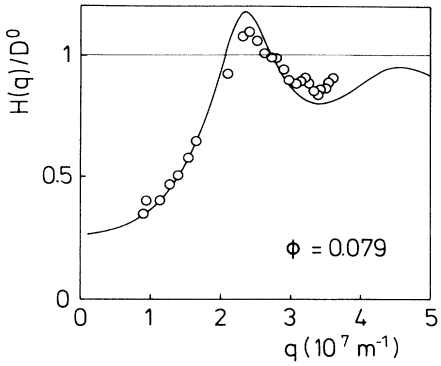

FIG. 11. Same as in Fig. 10, but with $\phi=0.079$.

well described by our pairwise additivity theory, including terms up to order r^{-11} (full line) and the renormalization approach (dashed line). The graphs resulting from both methods lie below the experimental data at small wave numbers. We note that the quantity $H(q)/D^0$, plotted in Fig. 10, has the limiting values $S(0)(D^{c,\text{short}}/D^0)$ for $q\to 0$ and $D^{s,\text{short}}/D^0$ for $q\to\infty$.

The difference between the two theoretical approaches and experiment at small q can be attributed to a similar difference between the experimental and theoretical $S(q)$. The renormalization approach predicts somewhat smaller values for $D^{c,\text{short}}$ and $D^{s,\text{short}}$ than pairwise additivity theory does. Numerically, it is found that $D^{s,\text{short}}/D^0=0.778$ and 0.860 by the renormalization method and the pairwise additivity theory, respectively. However, Genz and Klein mention that using the *ad hoc* assumption that $D^{s,\text{short}}/D^0=0.853$ in the renormalization approach reproduces the experimental data very well [11], and this value is quite close to our finding of 0.860. We also note that, according to Cichocki and Felderhof [21], a pure hard-sphere suspension with $\phi=0.101$, results in $D^{s,\text{short}}/D^0=0.815+O(\phi^2)$, where use of the expression $D^{s,\text{short}}/D^0=1-1.831\phi+O(\phi^2)$ has been made.

By including terms up to order r^{-7} within the two- and three-body hydrodynamic interaction, Beenakker and Mazur [22,24] obtained for hard-sphere suspensions an expression for $D^{s,\text{short}}$ to order ϕ^2, namely $D^{s,\text{short}}/D^0=1-1.73\phi+0.88\phi^2+O(\phi^3)$. This gives $D^{s,\text{short}}/D^0=0.834+O(\phi^3)$ (for $\phi=0.101$). We thus see that the short-time self-diffusion coefficient in the charged suspension is roughly equal to that predicted for the corresponding hard-sphere suspension. This has been experimentally verified by van Veluwen *et al.* [32] by comparing charged and uncharged silica suspensions.

In Fig. 11, the comparison between the pairwise additivity theory and the experimental data is also quite satisfactory for the suspension with $\phi=0.079$.

We have found the inclusion of terms up to order r^{-7} to be sufficient for the systems experimentally investigated by Philipse and Vrij. In fact, $H(q)$ calculated by including terms up to order r^{-11} is almost identical with the one containing only terms up to seventh order, even for a volume fraction as large as $\phi=0.101$; the largest difference between them is only 3%, occurring at $q=0$. This can be understood from Fig. 12, which shows the HNC radial distribution function $g(r)$ for several values of ϕ. The strong electrostatic repulsion keeps the particles apart from each other such that contact configurations are highly unlikely. Hence $g(r)$ is vanishingly small at distances $r\le 2.8a$, which are large enough to guarantee fast convergence of the far-field expansion.

VI. CONCLUSIONS

The objective of this work has been the investigation of the combined effect of hydrodynamic interaction and po-

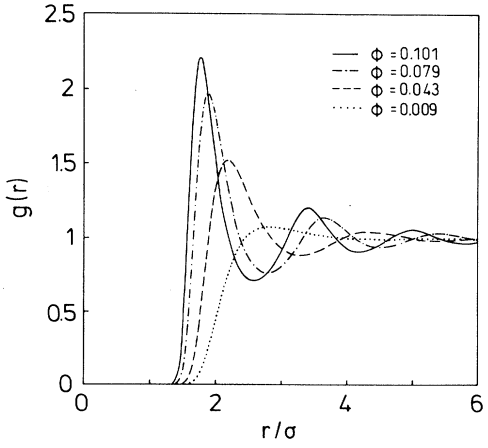

FIG. 12. HNC radial distribution function $g(r)$ corresponding to the charged silica suspensions of Philipse and Vrij. Volume fractions ϕ as given in the figure; all other parameters are the same as indicated in Fig. 8.

lydispersity on the short-time dynamics of charged suspensions at low and intermediate concentrations. We have used the multicomponent pairwise additivity theory to calculate the apparent wave-number-dependent diffusion coefficient $D_M(q)$, including terms up to order r^{-11} in the two-particle hydrodynamic far-field expansion. The intrinsic polydispersity in binary mixtures has been modeled by a bimodal Schulz distribution and the static correlation functions were calculated using the HNC closure.

The predictions of this pairwise additivity theory have been compared to DLS measurements of the first cumulant for dilute salt-free binary suspensions of charged polystyrene spheres. In this case only the leading term in the expansion of the mobilities in powers of the reciprocal distance between spheres, i.e., the so-called Oseen term of order r^{-1} is relevant, since the radial distribution functions are practically zero at distances r extending to several particle diameters. It was found that $D_M(q)$ was not affected by hydrodynamic interaction for wave numbers $q > q_{\max}$. At small wave number $q < q_{\max}$, however, a significant reduction of $D_M(q)$ by more than 10% was obtained as compared to $D_M^0(q)$, which is the apparent diffusion coefficient calculated without hydrodynamic interaction. This observation might explain the differences, found for certain dilute systems [9], between the structure factor $S_M^{\mathrm{SLS}}(q)$ determined by ordinary static light scattering and a "structure factor" $S_{M,0}^{\mathrm{DLS}}(q)$, which is obtained from a DLS experiment by assuming negligibly small hydrodynamic interaction. This latter structure factor is determined by rewriting Eq. (4.4) as

$$S_{M,0}^{\mathrm{DLS}}(q)=q^2\frac{H_M^0(q)}{\Gamma_M^{(1)}(q)} , \tag{6.1}$$

where

$$H_M^0(q)=\frac{1}{\overline{f^2}(q)}\sum_{\alpha=1}^{m} x_\alpha f_\alpha^2(q) D_\alpha^0 . \tag{6.2}$$

This corresponds to neglecting hydrodynamic interaction in Eq. (4.5). From the DLS experiment one uses $\Gamma_M^{(1)}(q)$ in Eq. (6.1) so that $S_{M,0}^{\mathrm{DLS}}(q)$ is fully determined. Any deviation of $S_{M,0}^{\mathrm{DLS}}(q)$ from $S_M^{\mathrm{SLS}}(q)$ is therefore an indication for the importance of hydrodynamic effects. The observation of $S_{M,0}^{\mathrm{DLS}}(q) > S_M^{\mathrm{SLS}}(q)$ for $q < q_{\max}$ found in Ref. [9] can now be understood, at least qualitatively. The correct expression for $S_M^{\mathrm{DLS}}(q)$ is

$$S_M^{\mathrm{DLS}}(q)=S_{M,0}^{\mathrm{DLS}}(q)\frac{D_M(q)}{D_M^0(q)} . \tag{6.3}$$

As can be seen from Fig. 3, the additional factor $D_M(q)/D_M^0(q) < 1$ for $q < q_{\max}$, which reduces the values of $S_{M,0}^{\mathrm{DLS}}(q)$ to $S_M^{\mathrm{DLS}}(q)$.

The effect of polydispersity on $D_M(q)$ and on the number-number diffusion coefficient $D_{NN}(q)$ was studied for increasing polydispersity by varying the standard deviations $s_{\mathrm{I,II}}$ of both components. It was observed that both hydrodynamic interaction and polydispersity give rise to a smaller value of $D_M(q)$ for $q < q_{\max}$, and that the oscillations in $D_M(q)/D_M^0(q)$ and $D_{NN}(q)/D_{NN}^0(q)$ are damped out with increasing polydispersity.

Our conclusions are consistent with recent observations by Cichocki and Felderhof [33]. They have calculated to first order in $\phi=(4\pi/3)\rho a^3$ the apparent short-time diffusion coefficient $D^{\mathrm{app}}(q)$ of a fictitious monodisperse effective hard-sphere suspension (EHS), in which the effective hard-core radius a^{eff} is assumed to be larger than the hydrodynamic particle radius a. The effective radius a^{eff} can be attributed to the strong repulsion between double layers in the case of charged suspensions. Using the far-field expansion of the two-particle diffusion tensors with stick boundary conditions, Cichocki and Felderhof find, in the case of EHS, that hydrodynamic interaction is negligibly small, provided that the effective hard-core radius is appreciably larger than the hydrodynamic one and provided that the scattering angles are not too small. They also find hydrodynamic corrections to the collective diffusion coefficient $D^{c,\mathrm{short}}=H(0)/S(0)$ to be important, the dominant correction coming from the Oseen part.

We have compared the pairwise additivity theory to recent light-scattering data of $H(q)$ for monodisperse charged silica suspensions at volume fractions up to $\phi\approx 0.1$. For these systems hydrodynamic interaction not only affects $D^M(q)$ at short wavelengths but also the short-time self diffusion coefficient such that $D^{s,\mathrm{short}}/D^0 < 1$. It was found that the additivity theory could fit the experimental data equally well as the renormalization method developed by Beenakker and Mazur does. Furthermore, it was sufficient for these systems to include terms up to r^{-7} in the expansions of the mobilities in terms of the reciprocal distance.

In our analysis we have restricted ourselves to charged suspensions with total volume fractions less than or equal to 0.1, and with ionic strengths small enough such that the radial distribution functions are practically zero at contact. Many charged suspensions studied so far fall into this regime. For these systems we anticipate the pairwise additivity theory to provide a semiquantitative description, albeit many-body effects have to be taken into account for a complete quantitative treatment of the problem.

At larger volume fractions however, many-body hydrodynamic effects are expected to be increasingly important, and one has to resort to schemes as proposed by Beenakker and Mazur. But an extension of their method to charged colloidal mixtures has not yet been worked out. Summarizing, we conclude that the "simple" pairwise additivity method proposed here is a useful tool to describe semiquantitatively the short-time dynamics in polydisperse charged suspensions at small to moderately large volume fractions.

ACKNOWLEDGMENTS

The authors are grateful to Dr. B. D'Aguanno for providing the multicomponent-HNC routine. Financial support from the Deutsche Forschungsgemeinschaft (SFB 306) is acknowledged.

APPENDIX

We first give the explicit expressions of the two particle hydrodynamic tensors $\mathbf{A}^{\alpha\beta}(\mathbf{r})$ and $\mathbf{B}^{\alpha\beta}(\mathbf{r})$ up to order r^{-11}, as obtained from general results by Jeffrey and Onishi [10]:

$$\mathbf{A}^{\alpha\beta}(\mathbf{r})=D_\alpha^0\left[-\frac{15}{4}\frac{a_\alpha a_\beta^3}{r^4}\mathbf{P}+\frac{15}{2}\frac{a_\alpha^3 a_\beta^3}{r^6}\mathbf{P}-\frac{1}{16}\frac{a_\alpha a_\beta^5}{r^6}(171+15\mathbf{P})\right.$$
$$-\frac{5}{4}\frac{a_\alpha^5 a_\beta^3}{r^8}(1+2\mathbf{P})+\frac{3}{32}\frac{a_\alpha^3 a_\beta^5}{r^8}(121+163\mathbf{P})-\frac{9}{8}\frac{a_\alpha a_\beta^7}{r^8}(1+\mathbf{P})-\frac{35}{16}\frac{a_\alpha^5 a_\beta^5}{r^{10}}(31+5\mathbf{P})$$
$$\left.-\frac{750}{8}\frac{a_\alpha^4 a_\beta^6}{r^{10}}\mathbf{P}+\frac{3}{8}\frac{a_\alpha^3 a_\beta^7}{r^{10}}(91+71\mathbf{P})-\frac{9}{8}\frac{a_\alpha a_\beta^9}{r^{10}}(1+\mathbf{P})\right]+O(r^{-12})\,, \tag{A1}$$

$$\mathbf{B}^{\alpha\beta}(\mathbf{r})=\frac{k_BT}{6\pi\eta}\left[\frac{3}{4r}(1+\mathbf{P})+\frac{1}{4r^3}[a_\alpha^2+a_\beta^2](1-3\mathbf{P})+\frac{75}{4}\frac{a_\alpha^3 a_\beta^3}{r^7}\mathbf{P}-\frac{15}{4}\frac{a_\alpha^3 a_\beta^3}{r^9}[a_\alpha^2+a_\beta^2]\mathbf{P}\right.$$
$$\left.+\frac{5}{8}\frac{a_\alpha^3 a_\beta^3}{r^{11}}[a_\alpha^4+a_\beta^4](71+5\mathbf{P})-\frac{1}{128}\frac{a_\alpha^5 a_\beta^5}{r^{11}}(5531+13\,943\mathbf{P})\right]+O(r^{-13})\,. \tag{A2}$$

where the projector $\mathbf{P}$ is defined by $\mathbf{P}=\hat{\mathbf{r}}\hat{\mathbf{r}}$. Note that $\mathbf{A}^{\alpha\beta}$ contains only even and $\mathbf{B}^{\alpha\beta}$ only odd powers in r^{-1}. Substituting these expressions into Eqs. (4.20) and (4.21) and performing the angular integrations leads to

$$D_\alpha^{s,\mathrm{short}}=D_\alpha^0\left[1+\sum_{\gamma=1}^{m}\phi_\gamma\left[-\frac{15}{4}a_\alpha\int_{a_\alpha+a_\gamma}^{\infty}dr\frac{g_{\alpha\gamma}(r)}{r^2}+\frac{a_\alpha}{8}[60a_\alpha^2-33a_\gamma^2]\int_{a_\alpha+a_\gamma}^{\infty}dr\frac{g_{\alpha\gamma}(r)}{r^4}\right.\right.$$
$$+\frac{a_\alpha}{32}[-200a_\alpha^4+597a_\alpha^2a_\gamma^2-144a_\gamma^4]\int_{a_\alpha+a_\gamma}^{\infty}dr\frac{g_{\alpha\gamma}(r)}{r^6}$$
$$\left.\left.+\frac{a_\alpha a_\gamma^2}{8}[-245a_\alpha^4-750a_\alpha^3a_\gamma+294a_\alpha^2a_\gamma^2-36a_\gamma^4]\int_{a_\alpha+a_\gamma}^{\infty}dr\frac{g_{\alpha\gamma}(r)}{r^8}\right]\right]\,, \tag{A3}$$

and $H_{\alpha\beta}^d$ can be written as a sum of four contributions,

$$H_{\alpha\beta}^d(q)=\rho_T(x_\alpha x_\beta)^{1/2}[\delta_O^{\alpha\beta}(q)+\delta_D^{\alpha\beta}(q)+\delta_S^{\alpha\beta}(q)+\delta_S^{*\alpha\beta}(q)]\,, \tag{A4}$$

where $\delta_O^{\alpha\beta}(q)=O(r^{-1})$, $\delta_D^{\alpha\beta}(q)=O(r^{-3})$, $\delta_S^{\alpha\beta}(q)=O(r^{-7})$, and $\delta_S^{*\alpha\beta}(q)=O(r^{-9},r^{-11})$. The four terms in Eq. (A4) are explicitly given by

$$\rho_T(x_\alpha x_\beta)^{1/2}\delta_O^{\alpha\beta}(q)=\tfrac{9}{2}a_\alpha D_\alpha^0\left[\frac{\phi_\alpha\phi_\beta}{a_\alpha^3a_\beta^3}\right]^{1/2}\left[\int_{a_\alpha+a_\beta}^{\infty}dr\,r[g_{\alpha\beta}(r)-1]\left[j_0(qr)-\frac{j_1(qr)}{qr}\right]-2Q_{\alpha\beta}\frac{j_1(2Q_{\alpha\beta})}{q^2}\right]\,, \tag{A5}$$

$$\rho_T(x_\alpha x_\beta)^{1/2}\delta_D^{\alpha\beta}(q)=\tfrac{3}{2}a_\alpha D_\alpha^0\left[\frac{\phi_\alpha\phi_\beta}{a_\alpha^3a_\beta^3}\right]^{1/2}[a_\alpha^2+a_\beta^2]\left[\int_{a_\alpha+a_\beta}^{\infty}dr[g_{\alpha\beta}(r)-1]\frac{j_2(qr)}{r}+\frac{j_1(2Q_{\alpha\beta})}{2Q_{\alpha\beta}}\right]\,, \tag{A6}$$

$$\rho_T(x_\alpha x_\beta)^{1/2}\delta_S^{\alpha\beta}(q)=\tfrac{225}{4}a_\alpha(a_\alpha a_\beta)^{3/2}D_\alpha^0(\phi_\alpha\phi_\beta)^{1/2}\int_{a_\alpha+a_\beta}^{\infty}dr\frac{g_{\alpha\beta}(r)}{r^5}\left[j_0(qr)-2\frac{j_1(qr)}{qr}\right]\,, \tag{A7}$$

$$\rho_T(x_\alpha x_\beta)^{1/2}\delta_S^{*\alpha\beta}(q)=-\tfrac{45}{4}a_\alpha D_\alpha^0(a_\alpha a_\beta)^{3/2}(\phi_\alpha\phi_\beta)^{1/2}(a_\alpha^2+a_\beta^2)\int_{a_\alpha+a_\beta}^{\infty}dr\frac{g_{\alpha\beta}(r)}{r^7}\left[j_0(qr)-2\frac{j_1(qr)}{qr}\right]$$
$$+\tfrac{3}{8}a_\alpha D_\alpha^0(a_\alpha a_\beta)^{3/2}(\phi_\alpha\phi_\beta)^{1/2}\int_{a_\alpha+a_\beta}^{\infty}dr\frac{g_{\alpha\beta}(r)}{r^9}\left\{(60[a_\alpha^4+a_\beta^4]-906a_\alpha^2a_\beta^2)j_0(qr)\right.$$
$$\left.-(50[a_\alpha^4+a_\beta^4]-\tfrac{13943}{8}a_\alpha^2a_\beta^2)\frac{j_1(qr)}{qr}\right\}\,. \tag{A8}$$

where $Q_{\alpha\beta}=q[a_\alpha+a_\beta]/2$, $\phi_\alpha=(4\pi/3)\rho_Tx_\alpha a_\alpha^3$, and j_n denote the spherical Bessel functions of order $n=0,1,2$.

[1] P. N. Pusey, in *Liquids, Freezing and Glass Transition: II,* 1989 Les Houches Lectures, edited by J. P. Hansen, D. Levesque, and J. Zinn-Justin (North-Holland, Amsterdam, 1991), pp. 763–942.
[2] R. B. Jones and P. N. Pusey, Annu. Rev. Phys. Chem. **42**, 137 (1991).
[3] W. Härtl, C. Segschneider, H. Versmold, and P. Linse, Mol. Phys. **73**, 541 (1991).
[4] B. V. R. Tata, R. Kesavamoorty, and A. K. Sood, Mol. Phys. **61**, 943 (1991).
[5] R. Krause, B. D'Aguanno, J. M. Mendez-Alcaraz, G. Nägele, R. Klein, and R. Weber, J. Phys. C **3**, 4459 (1991).
[6] B. D'Aguanno, R. Krause, J. M. Mendez-Alcaraz, and R. Klein, J. Phys.: Condens. Matter **4**, 3077 (1992).
[7] X. Qui, D. Ou-Yang, and P. M. Chaikin, J. Phys. (Paris) **49**, 1043 (1988).
[8] R. Krause, G. Nägele, J. L. Arauz-Lara, and R. Weber, J. Colloid Interface Sci. **148**, 231 (1992).
[9] R. Krause, J. L. Arauz-Lara, G. Nägele, H. Ruiz-Estrada, M. Medina-Noyola, R. Weber, and R. Klein, Physica A **178**, 241 (1991).
[10] D. J. Jeffrey and Y. Onishi, J. Fluid. Mech. **139**, 261 (1984).
[11] U. Genz and R. Klein, Physica **171**, 26 (1991).
[12] B. D'Aguanno and R. Klein, J. Chem. Soc. Faraday Trans. **87**, 379 (1991).
[13] B. D'Aguanno and R. Klein, Phys. Rev. A **46**, 7652 (1992).
[14] P. N. Pusey, H. M. Fijnaut, and A. Vrij, J. Chem. Phys. **77**, 4270 (1982).
[15] J. Happel and H. Brenner, *Low Reynolds Number Hydrodynamics* (Noordhoff International, Leiden, 1973).
[16] R. B. Jones and G. S. Burfield, Physica A **111**, 562 (1982), **111**, 577 (1982).
[17] S. Kim and S. J. Karrila, *Microhydrodynamics* (Butterworth-Heinemann, Boston, 1991).
[18] A. B. Bathia and D. E. Thornton, Phys. Rev. B **8**, 3004 (1970).
[19] W. van Megen, I. Snook, and P. N. Pusey, J. Chem. Phys. **78**, 931 (1983).
[20] B. U. Felderhof, J. Phys. A **11**, 929 (1978).
[21] B. Cichocki and B. U. Felderholf, J. Chem. Phys. **89**, 3705 (1988).
[22] C. W. J. Beenakker, Ph.D. thesis, Rijksuniversiteit Leiden, 1984.
[23] C. W. J. Beenakker and P. Mazur, Phys. Lett **98A**, 22 (1983).
[24] C. W. J. Beenakker and P. Mazur, Physica A **126**, 349 (1984); **120**, 388 (1983).
[25] R. B. Jones, Physica A **97**, 113 (1979).
[26] A. P. Philipse and A. Vrij, J. Chem. Phys. **88**, 6459 (1988).
[27] B. U. Felderhof, Physica A **89**, 373 (1977).
[28] P. Mazur and W. van Saarloos, Physica A **115**, 21 (1982).
[29] R. B. Jones and R. Schmitz, Physica A **149**, 373 (1988).
[30] W. van Megen, R. H. Ottewil, S. M. Owens, and P. N. Pusey, J. Chem. Phys. **82**, 508 (1985).
[31] I. Snook and W. van Megen, J. Colloid Interface Sci. **100**, 194 (1984).
[32] A. van Veluwen, H. N. W. Lekkerkerker, C. G. de Kruif, and A. Vrij, J. Chem. Phys. **87**, 4873 (1987).
[33] B. Cichocki and B. U. Felderhof, J. Chem. Phys. **94**, 556 (1991).